J ENDOVASC THER
2011;18:397–406

◆ EXPERIMENTAL INVESTIGATION ◆

Impact of Carotid Stent Cell Design on Vessel Scaffolding: A Case Study Comparing Experimental Investigation and Numerical Simulations

Michele Conti, MS[1,3]; Denis Van Loo, MS[2,5]; Ferdinando Auricchio, PhD[1]; Matthieu De Beule, PhD[3]; Gianluca De Santis, MS[3]; Benedict Verhegghe, PhD[3]; Stefano Pirrelli, MD[4]; and Attilio Odero, MD[4]

[1]Department of Structural Mechanics, Università degli Studi di Pavia, Italy. [2]Department of Physics and Astronomy, Centre of X-ray Tomography (UGCT). [3]BioMMeda (IBiTech) and [5]Department of Soil Management, Ghent University, Ghent, Belgium. [4]IRCCS Policlinico San Matteo, Pavia, Italy.

Purpose: To quantitatively evaluate the impact of carotid stent cell design on vessel scaffolding by using patient-specific finite element analysis of carotid artery stenting (CAS).
Methods: The study was organized in 2 parts: (1) validation of a patient-specific finite element analysis of CAS and (2) evaluation of vessel scaffolding. Micro-computed tomography (CT) images of an open-cell stent deployed in a patient-specific silicone mock artery were compared with the corresponding finite element analysis results. This simulation was repeated for the closed-cell counterpart. In the second part, the stent strut distribution, as reflected by the inter-strut angles, was evaluated for both cell types in different vessel cross sections as a measure of scaffolding.
Results: The results of the patient-specific finite element analysis of CAS matched well with experimental stent deployment both qualitatively and quantitatively, demonstrating the reliability of the numerical approach. The measured inter-strut angles suggested that the closed-cell design provided superior vessel scaffolding compared to the open-cell counterpart. However, the full strut interconnection of the closed-cell design reduced the stent's ability to accommodate to the irregular eccentric profile of the vessel cross section, leading to a gap between the stent surface and the vessel wall.
Conclusion: Even though this study was limited to a single stent design and one vascular anatomy, the study confirmed the capability of dedicated computer simulations to predict differences in scaffolding by open- and closed-cell carotid artery stents. These simulations have the potential to be used in the design of novel carotid stents or for procedure planning.

J Endovasc Ther. 2011;18:397–406

Key words: carotid artery, stent, cell design, vessel scaffolding, finite element analysis

Michele Conti has been partially supported by a PhD grant from MIUR (Ministero dell'Istruzione, dell'Università e della Ricerca, Italian Ministry of Education, University and Research) and by a Joint PhD scholarship from the University of Ghent (code: 01SF1308). Ferdinando Auricchio has been partially supported by the Cariplo Foundation through Project no. 2009.2822. Denis Van Loo has been partially supported by a PhD scholarship from the Research Foundation – Flanders (FWO, G.0100.08).

The authors have no commercial, proprietary, or financial interest in any products or companies described in this article.

Address for correspondence and reprints: Michele Conti, Università degli Studi di Pavia, Department of Structural Mechanics, Via Ferrata 1, 27100, Pavia, Italy. E-mail: *michele.conti@unipv.it*

The impact of stent cell design (i.e., closed vs. open) and vessel scaffolding on the clinical outcome of carotid artery stenting (CAS) is a matter of continued debate. Vessel scaffolding is determined by the free cell area, which is dependent upon the number and arrangement of bridge connectors. In closed-cell stents, adjacent ring segments are connected at every possible junction, while in open-cell stents, not all of the junction points are interconnected. Thus, a closed-cell stent design has a smaller cell area than its corresponding open-cell counterpart. In 2006, Hart et al.[1] analyzed a dual-center CAS database to identify patient and procedure parameters that have a negative impact on 30-day post CAS complications, i.e., stroke, death, and transient ischemic attack (TIA). Their analysis indicated that patients treated with closed-cell stents have a lower risk of experiencing adverse events compared to patients treated with open-cell design. The authors speculated that since TIAs are related to small particles passing through the stent mesh, the positive outcomes obtained using closed-cell stents are related to their smaller free cell area and thus to their intrinsically higher capability to scaffold and support the embologenic CAS lesion. One year later, Bosiers et al.[2] confirmed Hart's conclusions, showing that post-procedure complication rates are higher for the open-cell stent types, especially in symptomatic patients, and the rate increases with larger free cell area. Consequently, the authors speculated that stents with a smaller free cell area are better at containing plaque material behind the struts, resulting in significant differences in event rates compared to stents with large free cell areas.[3] Contrarily, Schillinger et al.[4] found no superiority of a specific carotid stent cell design with respect to neurological complications, stroke, or mortality risk after analyzing data from 10 European clinical centers. Theses contradictions and the different approaches used for data analysis have been further discussed,[5,6] highlighting the need of new dedicated studies.

The goal of the present study was to quantitatively evaluate the impact of carotid stent cell design on vessel scaffolding. For this purpose, an experimental approach was combined with computer simulations, i.e., finite element analysis (FEA). Micro-computed tomography (CT) images of an open-cell stent deployed in a patient-specific silicone artery phantom were compared with the corresponding FEA results. This simulation was repeated for the closed-cell counterpart. Subsequently, the circumferential stent strut distribution (inter-strut angle) was evaluated for both stent cell designs in different vessel cross sections as a measure of scaffolding.

METHODS

Silicone Model Construction

Several in vitro studies have used carotid artery silicone models to evaluate the efficacy of embolic protection devices and stent apposition.[7–12] Tanaka et al.[13] evaluated the conformability of 5 different types of self-expanding carotid stents implanted into simplified pulsatile perfused silicone models of a carotid bifurcation. Suzuki et al.[14] proposed the use of these models based on the images from clinical cases to simulate the endovascular procedure for interventional training.

To reproduce a realistic carotid artery anatomy model in the current study, a CT angiogram of the head and neck was acquired from an 83-year-old man using a Somatom Sensation Dual Energy scanner (Siemens Medical Solutions, Forchheim, Germany) with parameters of 1-mm slice thickness, a 512×512 matrix, and a 0.3-mm scan interval. The images were processed using Mimics software (version 13; Materialise, Leuven, Belgium) to obtain a stereolithographic (STL) description of the artery lumen (Fig. 1A,B). In this case, the common carotid artery (CCA) measured 7 mm in diameter and the internal carotid artery (ICA) 5.2 mm; a mild 24% stenosis (measured with the NASCET method) was present slightly above the bifurcation. The STL was used to fabricate an anatomically accurate silicone carotid artery (Advanced Vascular Models, Seaside, CA, USA); the model had variable wall thickness (Fig. 1C) to ensure a 5% radial compliance during a diastolic-systolic pressure cycle in the stenting region of interest.[15]

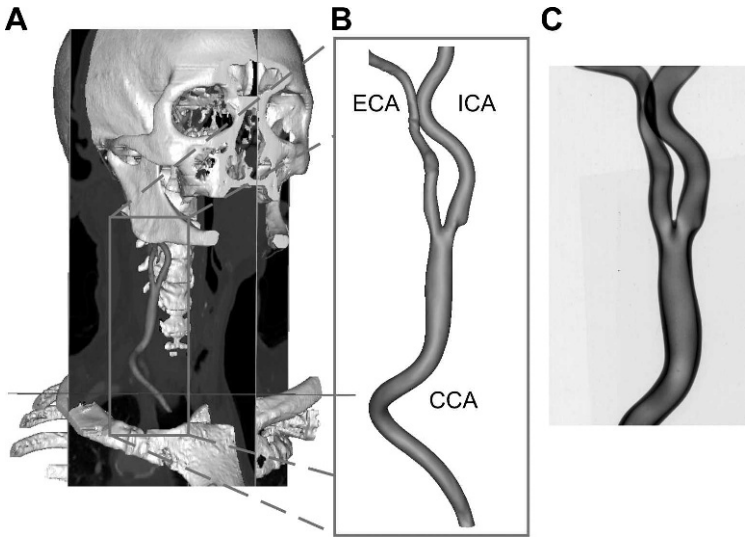

Figure 1 ◆ Construction of the carotid artery model. (**A**) 3D reconstruction of the cerebral vascular tree from a CT angiogram. (**B**) Surface describing the carotid artery lumen used to create the silicone artery. (**C**) Radiography of the silicone artery highlighting the non-uniform wall thickness. ECA: external carotid artery, ICA: internal carotid artery, CCA: common carotid artery.

Carotid Artery Finite Element Model

The silicone artery phantom had a variable wall thickness, so the finite element model of the vessel was created from a micro-CT scan with a resolution of 0.053 mm. To do this, the imported scan images were first segmented to limit the size of the model to 42 mm long (Fig. 2A) in order to reduce the computational cost. The segment was exported to a finite element solver (Abaqus/Explicit version 6.9; Dassault System, Providence, RI, USA) with a mesh defined by 73,322 elements [10-node modified tetrahedron with hourglass control (C3D10M)] and 134,092 nodes. The silicone was modeled as a hyperelastic material[16] using a second-order polynomial strain energy potential (U) defined as:

$$U = \sum_{i+j=1}^{2} C_{ij}(\bar{I}_1 - 3)^i(\bar{I}_2 - 3)^j + \sum_{i=1}^{2} \frac{1}{D_i}(J^{el} - 1)^{2i}$$

where C_{ij} and D_i are material parameters; I_1 and I_2 are the first and second deviatoric strain invariants, respectively; and J^{el} is the elastic volume ratio. To calibrate the material model, the stress-strain data (Fig. 2B) derived

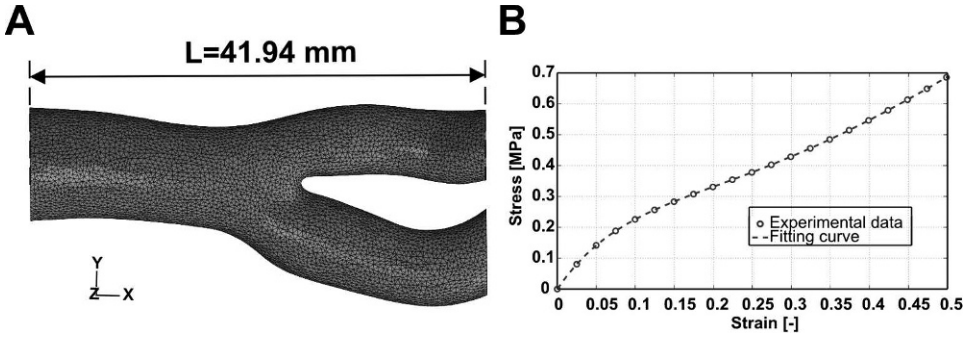

Figure 2 ◆ (**A**) 3D reconstruction (triangulated surface) of the silicone artery pre-stenting. (**B**) Adopted stress-strain curve for silicone material and related data fitting curve.

from a tensile test on silicone samples were fitted, obtaining the following non-null coefficients: $C10 = -2.40301$ MPa, $C01 = 3.02354$ MPa, $C20 = 0.456287$ MPa; $C11 = -1.72892$ MPa, and $C02 = 2.73598$ MPa.

Stent Finite Element Model

Realistic simulation of stent deployment requires an accurate representation of the actual stent geometry and its manufacturing process. For this experiment, a 9-mm ViVEXX Carotid Stent (C.R. Bard Angiomed GmbH & Co., Karlsruhe, Germany) was used. This stent is a straight, self-expanding open-cell design laser-cut from a low-profile nitinol tube.[17,18] The manufacturer sets the shape of the stent by expanding the laser-cut tube using a rigid expander; the expanded geometry is then thermally treated to set the superelastic properties. Finally, the superelastic expanded stent is crimped and packaged in the delivery system for subsequent release in the artery.

Since no data were available from the manufacturer on which to base a stent finite element model, the mesh was based on the micro-CT images of the stent crimped in the delivery catheter, assuming that this would accurately represent the laser-cut geometry. Thus, 2 micro-CT scans of the stent in the delivery system were acquired: one of the entire stent at a low resolution (20 μm) and another high-resolution (5 μm) scan of a portion of the stent (Fig. 3A). The dimensions of the stent (1.25-mm diameter and 0.190-mm strut thickness) were measured from the high-resolution micro-CT images using ImageJ (*http://rsbweb.nih.gov/ij/*). The planar slices obtained from the micro-CT scans were imported into Mimics to reconstruct the 3-dimensional (3D) configuration of the crimped stent (in STL format). The STL file was subsequently imported in pyFormex[19] and virtually unrolled, serving as a reference for the generation of the planar mesh of the stent; through appropriate geometrical transformations, the planar mesh led to the final laser-cut mesh.[20]

The finite element model of the laser-cut stent model consisted of 44,460 elements [8-node linear brick reduced integration with hourglass control (C3D8R)] and 82,890 nodes. The shape-setting process was simulated assuming that the stent diameter enlargement was driven by a rigid expander having an initial cylindrical shape (0.775-mm initial diameter and 33-mm length). The expander mesh consisted of 800 3D 4-node surface elements with reduced integration (SFM3D4R). The FEA controlled the expander by appropriate boundary conditions on its nodes, imposing a radial displacement of 3.9 mm in order to obtain an outer stent diameter of 9 mm. Prior to annealing, cold-worked nitinol behaves mechanically like metals such as aluminum or classic steel; consequently, for these simulations, nitinol was modeled as an elastoplastic material using the material parameters based on the work of Thériault et al.[18] A frictionless general contact algorithm was used to handle the interactions between the rigid cylinder and the stent.

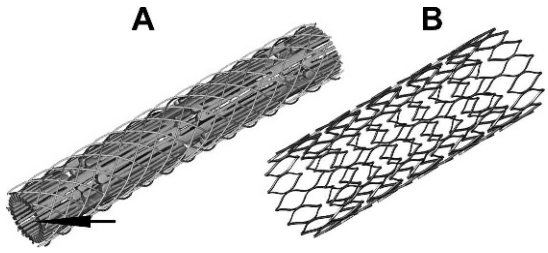

Figure 3 ◆ (**A**) 3D reconstruction of an 8.45-mm segment of the stent (arrow) within the catheter. (**B**) Finite element model of an open-cell stent after the shape-setting simulation.

To simulate stent deployment within the vessel, the nodal coordinates and element connectivity resulting from the shape setting simulations were re-imported (Fig. 3B), in this way modeling the annealing process. Then, to reproduce the superelastic material response, the Abaqus user material subroutine[21] of a superelastic model, originally proposed by Auricchio and Taylor[22,23] and based on the concept of generalized plasticity,[24] was used. The adopted nitinol constitutive parameters were obtained from the literature,[25] and the density was assumed to be 6.7 g/cm^3.

Stent Deployment: Experimental Test

The stent delivery system, previously lubricated to avoid friction, was introduced into the silicone artery phantom, which was restrained on a support (Fig. 4A). Several radiographic

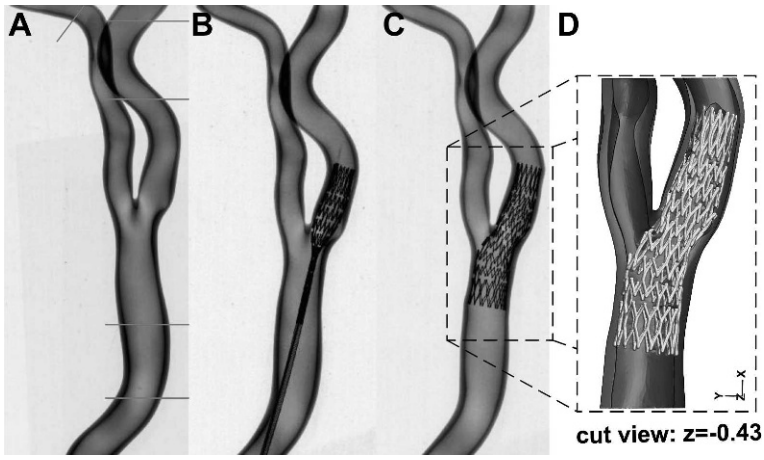

Figure 4 ◆ (**A**) Silicone artery: red lines indicate the location of restraints. (**B**) Silicone artery and partially-deployed stent. (**C**) Silicone artery and fully-deployed stent. (**D**) 3D reconstruction of the stent/artery configuration obtained from the micro-CT scan.

images were taken during the step-by-step deployment process (Fig. 4B,C). Finally, another micro-CT scan was performed with a resolution of 53 μm to obtain an accurate representation of the post-stenting artery/stent configuration. The initial and final micro-CT images of the silicone artery were processed using Mimics to obtain the 3D reconstruction depicted in Figure 4D. It is worth noting that self-expanding nitinol stents are designed to work in an isothermal environment at 37°C, but the test was performed at room temperature (~22°C), so a heating fan was used to induce full recovery of the expanded stent configuration and its complete deployment.

Stent Deployment: Numerical Simulation

To investigate the interaction between the stent and the patient-specific carotid artery model, a 2-step simulation procedure was performed.[26] In the first step, the diameter of the stent was decreased, simulating the loading of the stent into the delivery system. Subsequently, the stent inside the delivery sheath was placed into the target lesion; the retractable sheath was removed, allowing stent/vessel interaction and thus mimicking stent placement. The pre-stenting vessel centerline was used to guide stent positioning, and stent deformation was imposed by changing the retractable sheath profile using appropriate displacement boundary conditions on its nodes (these boundary conditions were determined as the difference between the starting and final sheath shape). The simulation was performed using Abaqus/Explicit as the finite element solver since the numerical analysis was characterized by non-linearity due to the material properties, large deformations, and complex contact problems. The general contact algorithm was used to handle the interactions between all model components; in particular, the contact between the stent and the delivery sheath was considered frictionless, but a friction coefficient of 0.2 was assumed between the stent and the vessel inner surface.

Postprocessing

To qualitatively validate the numerical simulation of stent deployment in the patient-specific carotid artery anatomy, the stent/vessel configuration obtained at the end of the simulation was compared with the 3D reconstruction of the experimental counterpart. From a quantitative point of view, the circumferential distribution of the stent struts at 3 defined vessel cross sections (i.e., CCA, bifurcation, and ICA) were compared by measuring the inter-strut angle between 2 consecutive struts. The center of gravity of the bounding box of the stent cross section was used as the center of the reference system enclosed between given adjacent struts.

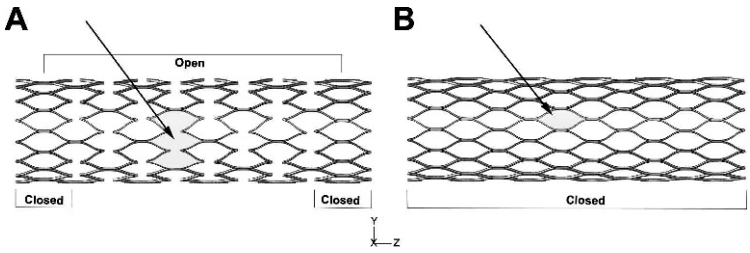

Figure 5 ◆ Details about the cell arrangement for the (**A**) open- and (**B**) closed-cell designs (the standard free cell area is indicated by arrows).

Evaluation of Vessel Scaffolding

The use of finite element modeling, and, in particular, of pyFormex as the preprocessing tool, can facilitate parametric analysis. In this study, this capability was used to increase the number of connectors in the original open-cell design from 5 to 15 (Fig. 5A) in order to define a closed-cell counterpart (Fig. 5B). The deployment simulation was then performed for the closed-cell stent. Both design variants of the stent strut distribution were evaluated in 5 different ICA cross sections, using the inter-strut angle as a measure of scaffolding.

RESULTS

Validation of Patient-Specific FEA of CAS

Figure 6 depicts the open-cell stent/vessel configuration for both the experimental test and the numerical analysis, while Table 1 displays the inter-strut angles for the section adjacent to the bifurcation. The qualitative comparison between the 3D reconstruction obtained from the micro-CT images and the numerical results agreed well, which was also confirmed by the substantial match between the measured inter-strut angles reported in Table 1. Figure 6 also shows the so-called fish-scale effect. Upon opening, the stent cell is bent due to the angulated bifurcation, causing misalignment and protrusion of the stent struts on the surface.

Vessel Scaffolding Evaluation

In Figure 7, the stent/vessel configuration obtained from the numerical analysis is depicted for both open-cell and closed-cell designs, while Figure 8 illustrates the inter-strut angle distribution at 5 ICA cross sections. In the closed-cell case, full connection between the rings maintained the tubular shape but restricted the stent's ability to accommodate to the irregular eccentric profile of the vessel cross section above the stenosis. The measured inter-strut angles (Table 2) and the strut distribution (Fig. 8) suggest that an open-cell design provides a higher maximum value in every section compared to the closed-cell design. This effect is particularly evident in the first 3 sections, corresponding to the vessel segment above the bifurcation, where the bending angle is higher and the vessel cross section irregular. Moreover, an open-cell design provides a less uniform circumferential distribution of the struts in every section, as demonstrated by a higher standard deviation of the inter-strut angle measurements.

DISCUSSION

Since complications following CAS are partially related to emboli passing through the stent struts, clinicians have focused their attention on the ability of a certain stent design (closed- vs. open-cell) to provide sufficient vessel scaffolding to avoid plaque protrusion. To quantitatively evaluate the impact of carotid stent cell design on vessel scaffolding, we computed the inter-strut angle distribution in different vessel cross sections as a measure of scaffolding for the 2 cell variants. In validating the CAS simulation, we found that the patient-specific FEA matched well with the experimental stent deployment, both qualitatively and quantitatively, demonstrating the reliability of our proposed numerical approach. Our results confirm the indications of Siewiorek and colleagues,[26] who recently discussed the

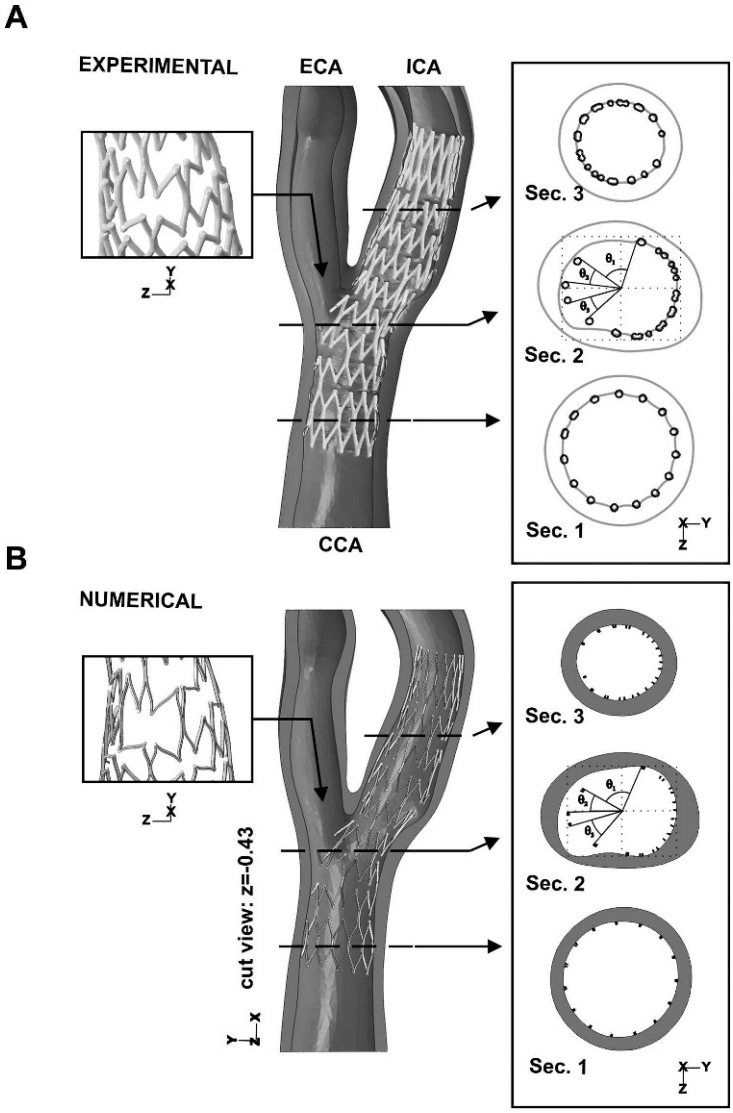

Figure 6 ◆ Comparison between experimental (**A**) and numerical (**B**) stent/vessel configurations. The figure highlights the strut position at 3 sections (1: x=10 mm, 2: x=19 mm, 3: x=30 mm) and the deformation of stent cells from a virtual view through the external carotid artery (ECA). The apparent mismatch of the stent strut thickness between the experimental and numerical results is due only to blooming artifacts in the micro-CT images.

TABLE 1
Finite Element Analysis of CAS: Inter-Strut Angles for Section 2 in Figure 6

	Inter-Strut Angles,°		
	θ_1	θ_2	θ_3
Experimental test	72.3	28.8	26.3
Numerical analysis	82.8	29.6	32.9
Difference	+10.5	+0.8	+6.6

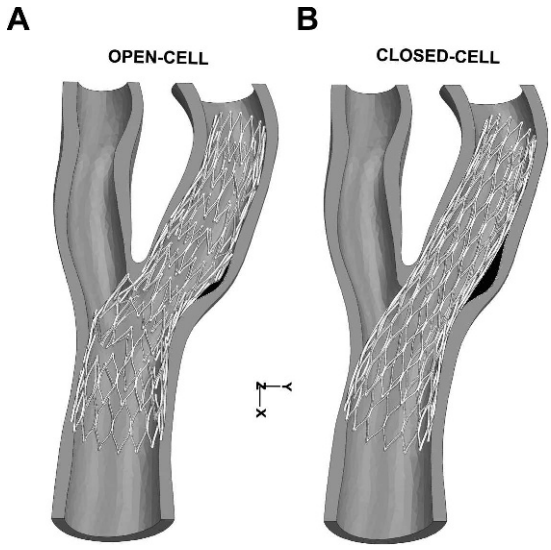

Figure 7 ◆ Stent/vessel configurations obtained by FEA of CAS for the (**A**) open-cell and (**B**) closed-cell designs. The gap between the stent and the vessel wall is in black.

clinical significance and technical assessment of stent cell geometry for CAS. The authors underlined the challenge of relating the post-procedure CAS events to a given stent design, but they indicated that FEA was an affordable tool to evaluate (new) stent configurations in a realistic environment.

The results of our vessel scaffolding evaluation indicate that a closed-cell design provides a more uniform circumferential strut distribution in every section of the stented segment compared to its open-cell counterpart. Moreover, the simulation of the open-cell stent deployment highlighted the so-called fish-scale effect[27,28]; whether this interaction of the stent struts with the vessel wall predisposes to restenosis or stent fracture is still a matter of concern.[29] As expected, the closed-cell design seemed to ensure superior vessel scaffolding, but it is necessary to underscore that its full strut interconnection reduced the stent's ability to accommodate to the eccentric profile of the vessel cross section, leading to a gap between the stent surface and the vessel wall.

Vessel scaffolding is not easily standardized or measured; it depends on several interrelated factors, but clearly, the size and type of the stent cell play primary roles. Typically,

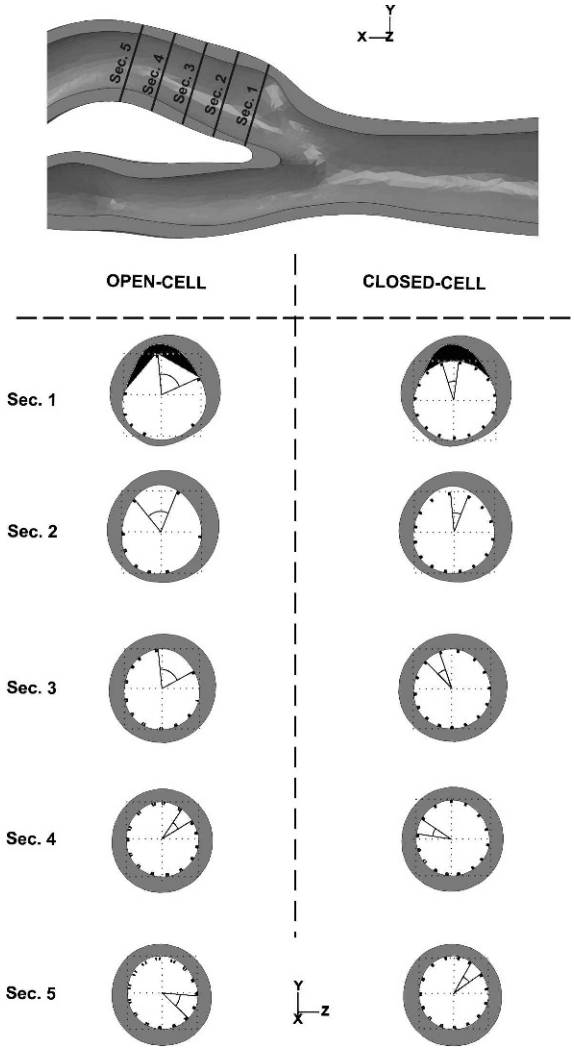

Figure 8 ◆ Cut views of 5 different vessel cross sections for both open-cell (left) and closed-cell designs (right). The section position is illustrated with respect to the pre-stenting vessel (top); the maximum inter-strut angle for each section is depicted. The gap between the stent and the vessel wall is in black.

vessel scaffolding is quantified by calculating the maximum free cell area of a given stent design in its free expanded configuration.[30] Although this measure is appropriate for comparing different designs, it is challenging to measure in vivo and does not take into account the actual configuration of a stent implanted in a tortuous carotid bifurcation. In the present study, we decided to use the inter-strut angle at different vessel cross sections as a measure of scaffolding since this method

TABLE 2
Open vs. Closed Cell: Inter-Strut Angles for the Sections Depicted in Figure 8

	Inter-Strut Angle, °	
	Open Cell	Closed Cell
Section 1	74 (46.3±28.2)	23.9 (19.6±2.1)
Section 2	69 (43±24)	26.5 (19.5±3.3)
Section 3	67.3 (24.7±14.7)	25.2 (19.5±3.6)
Section 4	25.8 (17.8±4.5)	25.1 (18.7±3.6)
Section 5	36.5 (18.3±5.2)	24.3 (18.5±2.7)

Data are presented as the maximum (mean ± standard deviation).

is closer to the actual clinical evaluation criteria. In fact, it is possible to assess stent apposition to the vessel wall by directly visualizing the stent strut distribution with intravascular ultrasound or optical coherence tomography.[31,32] Thus, future studies could compare the simulated prediction of strut distribution and these in vivo measurements.

Limitations

Although our numerical results were experimentally validated, some limitations affected this study. First, only one stent design in one specific anatomy was considered. Second, the degree of stenosis was low. To generalize our results, other devices should be tested with respect to other carotid artery anatomies. Although the degree of stenosis (24%) in this simulation did not meet the clinical indication for stenting, we believe that the vascular anatomy utilized was appropriate for the goal of the present study; clearly, future considerations of more severe degrees of stenosis would enforce the link between these simulations and clinical practice.

Conclusion

The present study assesses quantitatively the vessel scaffolding of a given stent design in a patient-specific carotid artery through experimentally-validated finite element analysis of CAS. The comparison of the stent strut distribution for open- vs. closed-cell designs of the same stent suggests that the closed-cell configuration provides superior scaffolding, but it has a reduced ability to conform to irregular or eccentric vessel cross-sectional profiles.

Though limited to a single stent design and one vascular anatomy, our study confirms the capability of dedicated computer simulations to predict differences in scaffolding by open- or closed-cell stents currently used for CAS. These simulations have the potential to be used in the design of novel carotid stents or for procedure planning purposes.

Acknowledgments: The authors would acknowledge Professor P. Segers (IBiTech-bioMMeda, Ghent University, Ghent, Belgium); Professor L. Van Hoorebeke (Department of Physics and Astronomy, Ghent University Centre for X-ray Tomography, UGCT); and A. Wachtmeester for their valuable support.

REFERENCES

1. Hart JP, Peeters P, Verbist J, et al. Do device characteristics impact outcome in carotid artery stenting? *J Vasc Surg*. 2006;44:725–731.
2. Bosiers M, de Donato G, Deloose K, et al. Does free cell area influence the outcome in carotid artery stenting? *Eur J Vasc Endovasc Surg*. 2007;33:135–141.
3. Bosiers M, Deloose K, Verbist J, et al. What practical factors guide the choice of stent and protection device during carotid angioplasty? *Eur J Vasc Endovasc Surg*. 2008;35:637–643.
4. Schillinger M, Gschwendtner M, Reimers B, et al. Does carotid stent cell design matter? *Stroke*. 2008;39:905–909.
5. Setacci C, de Donato G, Bosiers M. Two different studies on carotid stent cell design importance, or are we just saying the same thing? *Stroke*. 2008;39:e129.
6. Cremonesi A, Setacci C, Castriota F, et al. Carotid stent cell design: lack of benefit or lack of evidence? *Stroke*. 2009;39:e130.
7. Siewiorek G, Wholey M, Finol E. Vascular resistance in the carotid artery: an in vitro investigation of embolic protection filters. *J Vasc Interv Radiol*. 2008;19:1467–1476.
8. Siewiorek GM, Wholey MH, Finol EA. In vitro performance assessment of distal protection devices for carotid artery stenting: effect of physiological anatomy on vascular resistance. *J Endovasc Ther*. 2007;14:712–724.
9. Müller-Hülsbeck S, Stolzmann P, Liess C, et al. Vessel wall damage caused by cerebral protection devices: ex vivo evaluation in porcine carotid arteries. *Radiology*. 2005;235:454–460.

10. Müller-Hülsbeck S, Hüsler E, Schaffner S, et al. An in vitro analysis of a carotid artery stent with a protective porous membrane. *J Vasc Interv Radiol*. 2004;15:1295–1305.
11. Müller-Hülsbeck S, Jahnke T, Liess C, et al. Comparison of various cerebral protection devices used for carotid artery stent placement: an in vitro experiment. *J Vasc Interv Radiol*. 2003;14:613–620.
12. Müller-Hülsbeck S, Jahnke T, Liess C, et al. In vitro comparison of four cerebral protection filters for preventing human plaque embolization during carotid interventions. *J Endovasc Ther*. 2002;9:793–802.
13. Tanaka N, Martin J, Tokunaga K, et al. Conformity of carotid stents with vascular anatomy: evaluation in carotid models. *Am Soc Neuroradiol*. 2004;25:604–607.
14. Suzuki Y, Fujitsika M, Chaloupa J. Simulation of endovascular neurointervention using silicone models: imaging and manipulation. *Neurol Med Chir (Tokyo)*. 2005;45:567–573.
15. Ramesh R, Strope E, Price K, et al. Frequency dependent hysteresis of silicone and latex mock arteries used in stent testing. *Biomed Sci Instrument*. 2005;41:163–168.
16. Martins PA, Natal Jorge RM, Ferreira AJ. A comparative study of several material models for prediction of hyperelastic properties: application to silicone-rubber and soft tissues. *Strain*. 2006;42:135–147.
17. Rebelo N, Fu R, Lawrenchuk M. Study of a nitinol stent deployed into anatomically accurate artery geometry and subjected to realistic service loading. *J Mater Eng Perform*. 2009;18:655–663.
18. Thériault P, Terriault P, Brailovski V, et al. Finite element modeling of a progressively expanding shape memory stent. *J Biomech*. 2006;39:2837–2844.
19. pyFormex, A tool for generating, manipulating and operating on large geometrical models. Available at *http://pyformex.berlios.de/*. Last accessed January 15, 2011.
20. Mortier P, Van Loo D, De Beule M, et al. Comparison of drug-eluting stent cell size using micro-CT: important data for bifurcation stent selection. *EuroIntervention*. 2010;4:391–396.
21. Rebelo N, Walker N, Foadian H. Simulation of implantable stents. *Abaqus User's Conference*. 2001;143:421–434.
22. Auricchio F, Taylor R. Shape-memory alloys: modeling and numerical simulations of the finite-strain superelastic behavior. *Comput Methods Appl Mech Eng*. 1996;143:175–194.
23. Auricchio F, Taylor R. Shape-memory alloys: macromodeling and numerical simulations of the superelastic behavior. *Comput Methods Appl Mech Eng*. 1997;146:281–312.
24. Lubliner J, Auricchio F. Generalized plasticity and shape memory alloy. *Int J Solid Strc*. 1996;33:991–1003.
25. Kleinstreuer C, Li Z, Basciano C, et al. Computational mechanics of Nitinol stent grafts. *J Biomech*. 2008;41:2370–2378.
26. Auricchio F, Conti M, De Beule M, et al. Carotid artery stenting simulation: from patient-specific images to finite element analysis. *Med Eng Phys*. 2011;33:281–289.
27. Siewiorek GM, Finol EA, Wholey MH. Clinical significance and technical assessment of stent cell geometry in carotid artery stenting. *J Endovasc Ther*. 2009;16:178–188.
28. Wholey M, Finol E. Designing the ideal stent. *Endovascular Today*. 2007;6:25–34.
29. Varcoe RL, Mah J, Young N, et al. Prevalence of carotid stent fractures in a single-center experience. *J Endovasc Ther*. 2008;15:485–489.
30. Müller-Hülsbeck S, Schäfer PJ, Charalambous N, et al. Comparison of carotid stents: an in-vitro experiment focusing on stent design. *J Endovasc Ther*. 2009;16:168–177.
31. Okamura T, Garg S, Gutiérrez-Chico J, et al. In vivo evaluation of stent strut distribution patterns in the bioabsorbable everolimus-eluting device: an OCT ad hoc analysis of the revision 1.0 and revision 1.1 stent design in the absorb clinical trial. *EuroIntervention*. 2010;5:932–938.
32. Opolski M, Pracon R, Mintz G, et al. Relation of drug-eluting stent strut distribution to stent thrombosis in coronary arteries. *Am J Cardiol*. 2009;104:343–348.